PAPER

Check for updates

Tuning N-heterocyclic carbene wingtips to form electrochemically stable adlayers on metals†

Isabel M. Jensen,‡[a] Vincent Clark, [ID] ‡[b] Harper L. Kirby,[a] Netzahualcóyotl Arroyo-Currás [ID] *[bc] and David M. Jenkins [ID] *[a]

Self-assembled monolayers (SAMs) are employed in electrochemical biosensors to passivate and functionalize electrode surfaces. These monolayers prevent the occurrence of undesired electrochemical reactions and act as scaffolds for coupling bioaffinity reagents. Thiols are the most common adlayer used for this application; however, the thiol-gold bond is susceptible to competitive displacement by naturally occurring solvated thiols in biological fluids, as well as to desorption under continuous voltage interrogation. To overcome these issues, N-heterocyclic carbene (NHC) monolayers have been proposed as an alternative for electrochemical biosensor applications due to the strong carbon–gold bond. To maximize the effectiveness of NHCs for SAMs, a thorough understanding of both the steric effects of wingtip substituents and NHC precursor type to the passivation of electrode surfaces is required. In this study, five different NHC wingtips as well as two kinds of NHC precursors were evaluated. The best performing NHC adlayers can be cycled continuously for four days (over 30 000 voltammetric cycles) without appreciably desorbing from the electrode surface. Benchmark thiol monolayers, in contrast, rapidly desorb after only twelve hours. Investigations also show NHC adlayer formation on other biosensor-relevant electrodes such as platinum and palladium.

Introduction

Electrochemical biosensors allow real-time, *in vivo* molecular monitoring directly within the human body.[1,2] This feat has been successfully demonstrated commercially and in the clinic by the continuous glucose monitor (CGM), which significantly improved the quality of life of Type 1 diabetics.[3] Additionally, sensing approaches leveraging the affinity of nucleic acids for reversible molecular recognition offer the promise to vastly expand the scope of molecules that can be sensed continuously *in vivo*.[4–8] These newer sensors often consist of electrodes modified *via* self-assembled alkylthiol monolayers (SAMs) on gold, which are leveraged to block non-specific molecular interactions with the electrode, prevent the occurrence of undesired electrochemical reactions, and provide a scaffold to which biorecognition elements (*e.g.*, nucleic acids, antibodies)

can be covalently attached. To date, various types of SAM-based sensors have been shown to work *in vivo* with a wide variety of analytes such as proteins,[9–12] pharmaceuticals,[13] and metabolites,[14,15] highlighting their incredible potential as broadly applicable molecular monitoring platforms.

Despite their promise, one of the greatest challenges that SAM-based sensors face is their short operational stability.[16] For example, nucleic acid aptamer-based sensors have a limited duration of hours before they begin to deteriorate, as opposed to the more biomedically relevant timescale of days or weeks.[17,18] The weakest link for these biosensors is the chemical bond between the electrode surface and the SAM.[19] Specifically, previous studies by us and others have shown that voltage-induced desorption[17,20] and competitive displacement are the driving causes of alkylthiol-based SAM decay in biofluids.[20–22] Thus, to extend the longevity of SAM-based electrochemical biosensors to physiologically relevant timescales, and improve the commercialization of these technologies, we must first address the weakness of the metal–SAM bond.

N-heterocyclic carbenes (NHCs) are an emerging alternative to thiols that form incredibly stable SAMs on gold.[23,24] NHC monolayers show stability under a wide variety of temperatures, pH, and even in biofluids.[23,25–30] We and others have noted NHCs' stability under continuous electrochemical interrogation,[25,31–34] which is the critical weak-point of thiols used for electrochemical biosensor applications. Their value for electrochemical sensing is

[a] *Department of Chemistry University of Tennessee Knoxville Knoxville, TN 37996, USA. E-mail: jenkins@ion.chem.utk.edu*

[b] *Chemistry-Biology Interface Program Johns Hopkins University Baltimore, MD 21218, USA*

[c] *Department of Pharmacology and Molecular Sciences Johns Hopkins University School of Medicine Baltimore, MD 21205, USA. E-mail: netzarroyo@jhmi.edu*

† Electronic supplementary information (ESI) available: Detailed electrochemical and synthetic methods as well as additional characterization, spectra and electrochemical data. See DOI: https://doi.org/10.1039/d4ma00648h
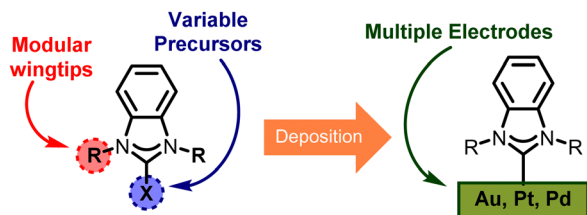
‡ Equally contributing authors.

Fig. 1 Utilizing the modularity of NHCs by varying wingtip composition and precursor type to form self-assembled monolayers on a variety of electrode surfaces.

already becoming apparent as Crudden reported a preliminary application of NHC SAMs for electrochemical sensing of the measles virus.[31] However, many questions remain regarding the impact of NHCs wingtip position and precursor species—both of which are known to impact monolayer organization and monolayer quality—on electrochemical stability.[24,35–37] To date, there have been neither comparative studies of wingtip effects or deposition methods for electrochemical stability of NHCs, nor what effects they may have on SAM longevity under continuous interrogation.

In this manuscript, we have undertaken a systematic approach to investigate the effects that wingtip and NHC precursor species have on electrode passivation and monolayer longevity (Fig. 1). Five different wingtip sizes were evaluated across NHCs ranging from methyl to *tert*-butyl along with two distinct approaches to NHC deposition, from a triflate salt or NHC–CO_2 adduct. We evaluated the performance of the monolayers for electrode passivation *via* the monitoring of capacitive currents in cyclic voltammetry compared to benchmark thiol mercaptohexanol (MCH) SAMs. The best performing NHCs were then subjected to continuous electrochemical interrogation over 96 hours to evaluate longevity of monolayers and showed no significant long-term degradation. In contrast, MCH-based SAMs decayed over just 12 hours. Finally, we compared the best-performing NHCs and evaluated them across different noble metal electrodes, with the goal of expanding their use to electrode surfaces other than gold.

Results and discussion

We first investigated the effects of steric hindrance of NHC wingtips on the electrochemical passivation of gold electrodes. To this end, we prepared NHCs with wingtips of five different sizes ranging from methyl to *tert*-butyl. Since small NHC wingtips, such as methyl, cannot form NHC–CO_2 adducts, we turned to the formation of triflate salts of benzimidazoliums, which have been reported to form stable adlayers on gold (Fig. 2A, green background).[31,33] Starting from the same precursor for depositions allows for a direct comparison of the wingtip effects on the adlayers formed. We compared these triflate salts to NHC–CO_2 adducts since they are well-established for the formation of stable and dense monolayers on gold.[38–42] These were the isopropyl and *tert*-butyl wingtips compounds (Fig. 2A, purple background). To maintain clarity for deposition procedures on
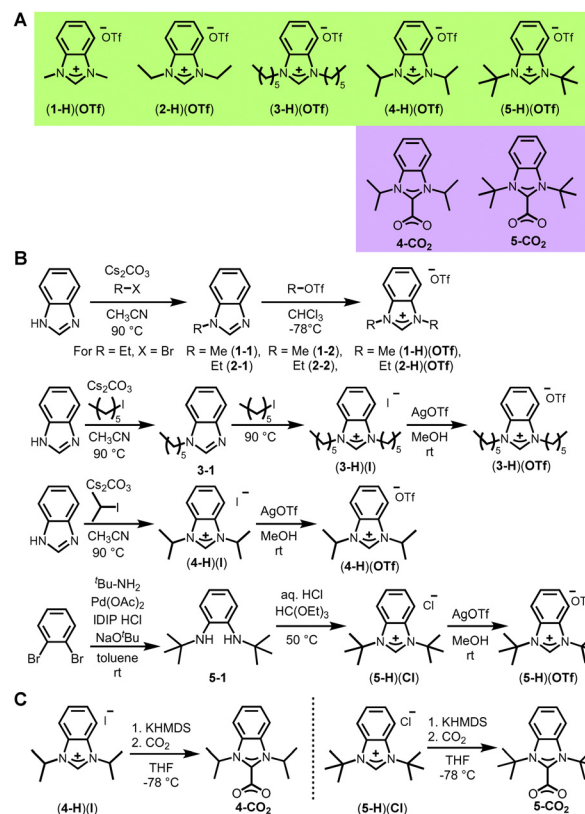

Fig. 2 Synthetic routes of benzimidazolium trifluoromethanesulfonate (triflate) salts and NHC–CO_2 adducts. (A) Summation of all NHC precursor structures evaluated for the electrochemical passivation of gold electrodes. Green and purple colors are used throughout the manuscript to describe which type of NHC precursor is applied to an electrode. (B) The distinct paths for synthesis of triflate (OTf$^-$) salts. (C) Synthesis paths of two NHC–CO_2 adduct.

electrode surfaces, the NHCs will continue to have these background colors in figures throughout the text.

Although the benzimidazoliums for each of the five wingtips have been previously prepared, most of them had not been synthesized with the key triflate counteranion. The methyl- and isopropyl-winged benzimidazolium triflate salts—(1-H)(OTf) and (4-H)(OTf), respectively—were synthesized as previously published in literature (Fig. 2B).[43,44] For (1-H)(OTf), we first synthesized the alkyl triflate MeOTf and then added the alkyl benzimidazole (1-1), with the triflate remaining as the counteranion to the benzimidazolium. The ethyl-winged benzimidazolium triflate, (2-H)(OTf), was synthesized in this same manner (Fig. 2B). The first ethyl substituent was added *via* addition of 1-ethyl iodide to benzimidazole in the presence of cesium carbonate as a base to yield 2-1. To synthesize the final triflate salt, 2-1 was first dissolved in dichloromethane and cooled to −78 °C. Ethyl triflate (2-2, prepared by the method of Yoshida[45]) was diluted with dichloromethane and slowly added to the stirring solution of 2-1, which we stirred for one hour before the bath was removed, and the reaction mixture was allowed to warm to room temperature overnight while stirring. All volatiles were removed, and the solids redissolved in dichloromethane before triturating with cold diethyl ether (at 0 °C), which gave

the product **(2-H)(OTf)** in 93% yield as a pale purple solid. The remaining two triflate salts with *n*-hexyl and *tert*-butyl wingtips required different synthetic approaches. The previous route that was successful for **(2-H)(OTf)** surprisingly did not work for preparation of the *n*-hexyl-winged benzimidazolium triflate **(3-H)(OTf)**. Instead, to prepare **(3-H)(OTf)**, we first synthesized the di-*n*-hexyl-benzimidazolium iodide salt **(3-H)(I)** *via* the stepwise addition of two *n*-hexyl wings using 1-iodohexane (Fig. 2B).[46] We then carried out an anion metathesis reaction with silver triflate in methanol to precipitate silver bromide and quantitatively yield the dark orange hexyl-winged benzimidazolium triflate **(3-H)(OTf)**. A key distinction between **(3-H)(I)** and **(3-H)(OTf)** is the difference in chemical shift values between their ^1H NMR spectra, with the benzimidazolium proton resonances ranging from 10.96 to 9.81 ppm (Fig. S45 and S23, respectively, ESI†). For **(4-H)(OTf)** we followed the previously published method of anion exchange with silver triflate, first synthesizing **(4-H)(I)** directly from benzimidazole,[42] then proceeding with the anion exchange in methanol.[43]

For the *tert*-butyl wingtip NHC, the first step was the formation of *N,N'*-di-*tert*-butyl-1,2-diaminebenzene (**5-1**) from *o*-dibromobenzene and *tert*-butyl amine *via* a Buchwald-Hartwig amination reaction (Fig. 2B).[47] A ring-closing reaction with ethyl orthoformate and **5-1** under acidic conditions (with HCl) yielded *N,N*-di-*tert*-butyl-benzimidazolium chloride **(5-H)(Cl)**.[48] The counteranion for **(5-H)(Cl)** was then converted to the triflate using silver triflate to give the faintly pink **(5-H)(OTf)** in 88% yield.

In addition to the benzimidazolium triflate salts, we prepared two NHC–CO_2 adducts for comparison. The synthesis of the isopropyl wingtipped NHC–CO_2 adduct **4-CO_2** proceeded *via* an adapted procedure published by our group (Fig. 2C).[42] The novel *tert*-butyl wingtip NHC–CO_2 adduct, **5-CO_2**, was synthesized utilizing a similar procedure. Deprotonation of *N,N*-di-*tert*-butyl-benzimidazolium chloride **(5-H)(Cl)** was accomplished with potassium hexamethyldisilazane in THF at −78 °C to afford the free carbene. The solution was then filtered over Celite to remove potassium chloride. The solution with free carbene (**5**) was then cooled to −70 °C in a Strauss tube with a stir bar and attached to a Schlenk line. The line and headspace of the tube was evacuated, after which carbon dioxide gas was added. The addition of CO_2 gas led to the gradual precipitation of a white solid, **5-CO_2**. The solution was then cooled to −30 °C in a glovebox and triturated with cold diethyl ether. A fine white powder of **5-CO_2** was then collected by filtration on a fine frit in 5% yield. Compound **5-CO_2** has very poor solubility in all non-protic solvents; however, we were able to obtain its ^1H NMR spectrum in dry $CDCl_3$ that showed the absence of the key benzimidazolium proton (Fig. S35, ESI†).

The method of deposition onto the electrodes is critical and was modified from our previous reports to enhance reproducibility and reduce contamination between NHCs. We previously demonstrated that **(4-H)(OTf)** could passivate the surface of gold electrodes to a similar extent as the benchmark MCH.[33] To complete that study, we formed adlayers *via* deposition of the NHCs from methanolic solutions of their triflate salts over 4 h

at room temperature, similar to benchmark MCH deposition methods.[49] Here, we employed a vacuum oven (Thermo Scientific) to deposit the carbenes from 1 mM methanolic solutions at high temperature (120 °C) and reduced pressure (10 inHg) over a shorter period of 25 min to ensure sufficient coverage of the electrode surface. To prevent NHC cross contamination, we coated the vacuum oven with aluminum foil that was disposed of when switching between NHC ligands. Additionally, we observed that NHCs absorb so strongly to the gold electrode that they cannot be removed using standard protocols typically employed to remove thiol-based monolayers. To address this second challenge, we implemented a more aggressive chemical and electrochemical cleaning strategy (documented in detail in the Electrochemical methods section of the ESI†), that achieves complete electrode regeneration prior to new NHC depositions.

To understand the passivation effect of the various NHC ligands on gold electrodes, we note that the electrode–electrolyte interface can be represented as a parallel-plate capacitor, in which the electrode and the electrolyte represent the capacitor plates, and any adlayers in between represent the dielectric.[50] Following this model, densely packed and tall monolayers will decrease electrode capacitance because they decrease the permittivity of the dielectric and increase the distance between the plates. Conversely, poorly packed and shorter monolayers can increase electrode capacitance. Finally, the absence of an adlayer will result in the largest capacitance of the system. These effects are illustrated in Fig. 3A for a gold electrode and a benchmark monolayer of 6-mercaptohexanol. In the absence of the monolayer (yellow trace), the capacitive current of the gold electrode (5.9 ± 1.9 μA cm^{-2}) is approximately four times greater than when the thiol monolayer is formed (1.2 ± 0.3 μA cm^{-2}). These measurements offer a quantitative reference for comparisons to NHCs on their passivation of gold electrodes.

We performed serial investigation of NHC-coated gold electrodes *via* cyclic voltammetry measurements every 11 s for 24 h. By doing so, we could measure capacitive currents at $t = 0$ immediately after NHC deposition, and also monitor their stability during continuous voltage modulation. Five different NHC wingtips were investigated including methyl, ethyl, *n*-hexyl, isopropyl, and *tert*-butyl (Fig. 3B–F). We selected triflate salts for these NHCs based on multiple prior reports that proposed them for direct adlayer formation on gold.[31,33] Following NHC deposition, electrodes were cycled from −0.1 V to 0.3 V (*vs.* Ag|AgCl) in phosphate-buffered saline. We previously determined that scanning within this voltage window prevents voltage-induced desorption of chemisorbed thiol or NHC adlayers.[33]

All NHCs adsorbed strongly onto gold electrodes (Fig. 3B–F). Notably, we observed significant differences in capacitive currents caused by the structural differences of the NHC wingtips. NHCs with small wingtips such as methyl (Fig. 3B, 3.1 ± 0.8 μA cm^{-2}) and ethyl (Fig. 3C, 3.9 ± 0.7 μA cm^{-2}) achieved electrode surface passivation within a factor of 3 of that of 6-mercaptohexanol (Fig. 3A, 1.2 ± 0.3 μA cm^{-2}). Crucially, their passivation did not change after 8000 voltammetric cycles. In contrast, *n*-hexyl (Fig. 3D), isopropyl (Fig. 3E), and *tert*-butyl (Fig. 3F) wingtipped NHCs generated adlayers that presented transitionary peaks at
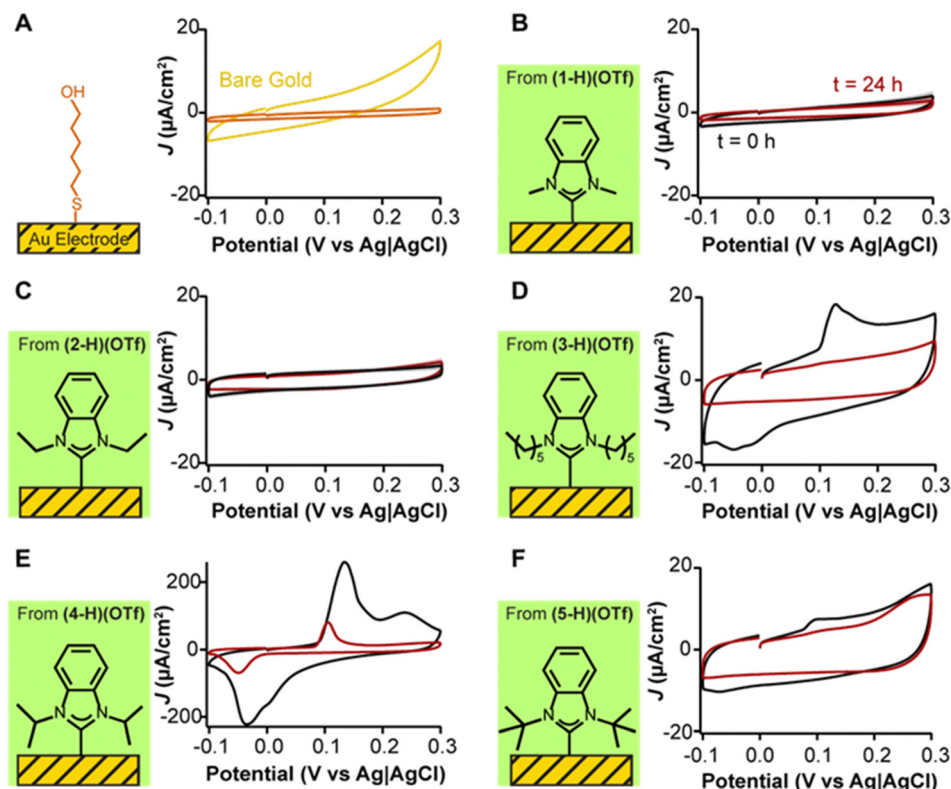
Fig. 3 Effect of alkanethiol and NHC deposition on the voltammetry of gold electrodes. (A) Mercaptohexanol (MCH) deposition (orange trace) results in dampening of capacitive currents relative to bare gold electrodes (yellow trace). (B) NHC 1 from **(1-H)(OTf)** and (C) NHC 2 from **(2-H)(OTf)** passivate the electrode to a similar extent relative to MCH. NHCs with bulkier, more hydrophobic wingtips: (D) NHC 3 from **(3-H)(OTf)**, (E) NHC 4 from **(4-H)(OTf)**, and (F) NHC **5** from **(5-H)(OTf)**, all form adlayers that show transitionary capacitive peaks at $t = 0$ h (black traces) which progressively decrease in magnitude upon repeated voltammetric cycling (red traces). Cyclic voltammograms are shown as current density ($\mu A\ cm^{-2}$), normalized to the microscopic surface area of the electrodes. The voltage scanning rate was 0.1 V s^{-1}. Red traces are the last measurement of 8000 total scans, interrogated every 10 s for 24 h. Traces were chosen to illustrate the capacitive effects. Data averaging four replicates plus their standard deviation are included in Fig. S2–S6 (ESI†).

voltages above 0.1 V, which showed reversibility at voltages below −0.05 V. These voltammetric features decreased in current magnitude upon continuous interrogation, with complete disappearance in the case of the *n*-hexyl wingtipped NHC after 24 h of continuous scanning. However, even after 24 h, baseline capacitive currents (hexyl: 8.5 ± 3.1 $\mu A\ cm^{-2}$, isopropyl: 19.6 ± 9.8 $\mu A\ cm^{-2}$, *tert*-butyl: 8.6 ± 4.6 $\mu A\ cm^{-2}$) did not show electrode passivation to the same extent as adlayers made with NHCs having methyl and ethyl wingtips.

Given that NHCs are not redox active at the voltages shown in Fig. 3, we propose that the redox peaks seen for the hexyl, isopropyl, and *tert*-butyl wingtips are due to silver ions remaining from the anion exchange conducted to replace iodide for triflate (Fig. 2B).[51–53] Unfortunately, synthetic difficulty to create the triflate salts significantly increases if silver halides are not used.

To further demonstrate that the voltammetric peaks we observed are due to silver contamination, we prepared fresh adlayers of the NHC with isopropyl wingtips (from Fig. 3E) and carried out cyclic voltammetry measurements in phosphate-buffered saline containing different anionic species. As expected,[54,55] the silver stripping and deposition peaks are a function of anion identity (Fig. 4A–F), with the largest features being observed for moderately adsorbing anions of large ionic

radius such as phosphate (Fig. 4A), chloride (Fig. 4C), and bromide (Fig. 4D) onto the silver contaminants. Iodide contributed to a large capacitive current but its silver complex did not undergo redox processes within the voltage window used (Fig. 4E). Fluoride anions, which have a significantly smaller ionic radius relative to the other halides, generated redox peaks that were one order of magnitude smaller (Fig. 4B + inset). It is likely that the lower currents observed in the presence of fluoride reflect slower redox kinetics at the electrode surface. A final experiment conducted with nitrate, a weakly adsorbing anion, showed negligible peaks (Fig. 4F + inset). However, adding chloride to the nitrate-containing solution slowly caused the reappearance of the silver redox peaks (Fig. S12, ESI†). Overall, these results provide strong evidence that silver cross-contamination from anion exchange reactions during NHC synthesis can drastically affect monolayer organization, packing and electrochemical behavior.

To avoid silver carry over from NHC syntheses to monolayer formation, we synthesized NHC–CO_2 adducts which do not require anion exchange. NHC–CO_2 adducts have been established to well-characterized monolayer formation and also displayed this behavior under electrochemical cycling.[25,32,41] We compared **4-CO_2** and **5-CO_2** to the previously evaluated
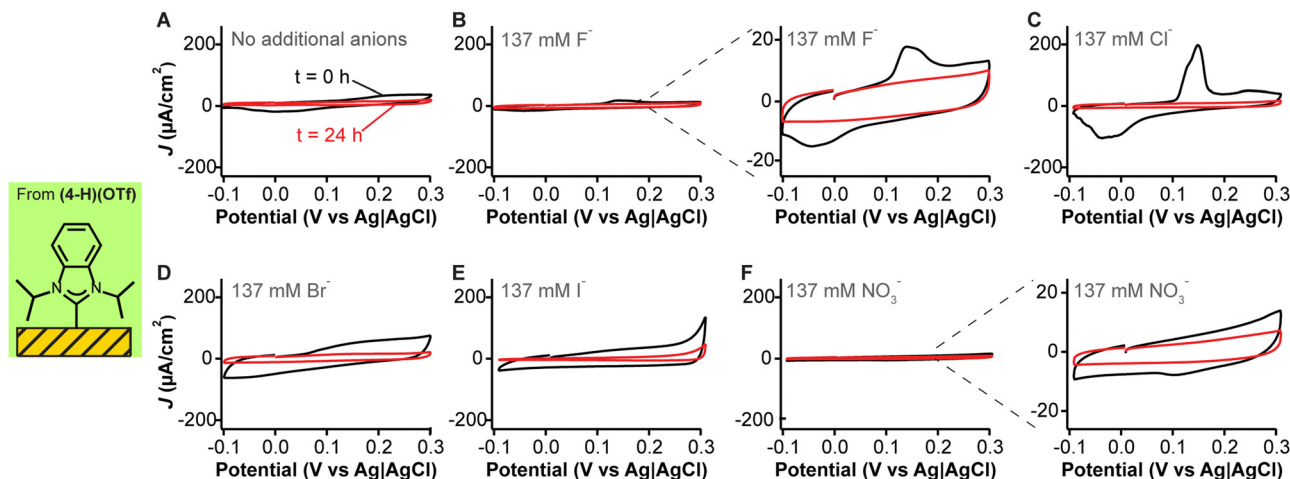
Fig. 4 Anion effects on the capacitive transitions of NHCs with isopropyl wingtips. These cyclic voltammograms correspond to the first (black traces) and last (red traces) cycles out of 8000 measurements in either (A) phosphate buffer alone (11.8 mM PO_4^{3-}), or phosphate-buffered saline containing 137 mM of (B) fluoride, (C) chloride, (D) bromide, (E) iodide or (F) nitrate anions. Traces were chosen to illustrate the capacitive effects. Data averaging four replicates plus their standard deviation are included in Fig. S7–S11 (ESI†).

(4-H)(OTf) and (5-H)(OTf). We deposited 4-CO₂ and 5-CO₂ on gold electrodes *via* the same method in a vacuum oven. In stark contrast to the deposition of the triflate salts, we observed no redox peaks *via* cyclic voltammetry for 4-CO₂ and 5-CO₂ (Fig. 5), with a concomitant reduction in voltammetric capacitance indicating the presence of well-formed monolayers passivating the electrode. Additionally, voltammetry performed on 4-CO₂ but in the presence of silver ions showed redox peaks similar to those seen in Fig. 3E and 4C (data shown in Fig. S13, ESI†), further confirming the redox peaks were due to silver contamination. These results demonstrate that NHCs synthesized as CO_2 adducts have higher purity relative to their triflate analogs and can quickly decarboxylate upon reacting with the gold surface to form a clean chemisorbed self-assembled monolayer.

While the silver contamination partially hinders a comprehensive evaluation, capacitive currents are related to binding mode and packing of the NHCs on the gold electrode. These, in turn, are dictated by the size of the NHCs' wingtips. We observe that for the two non-silver contaminated triflate species, the smaller methyl-winged NHC deposited from (1-H)(OTf) performs slightly better than the ethyl-winged NHC deposited from (2-H)(OTf) when evaluating the reduction in capacitive current (Fig. 3B and C, respectively). This result is consistent with ours and other previous studies that show the methyl winged NHCs lie flat on gold surfaces and pack very efficiently.[35–37] Similarly, for the CO_2-adducts, we note that the isopropyl-winged 4-CO₂ performs better than bulkier counterpart *tert*-butyl winged 5-CO₂ (Fig. 5A and B, respectively). As the wingtip size increases, NHCs are more likely to stand up on gold surfaces, which changes their packing mode.[23,24] Isopropyl wingtips, in particular, have been found to be highly effective at creating self-assembled monolayers on gold surfaces.[25,27,38,56]

A requirement for electrochemical sensors in medicine is long term stability. Since the adlayers achieving greatest gold electrode passivation were (1-H)(OTf) (Fig. 2B) and 4-CO₂ (Fig. 5A), we tested these two NHCs against mercaptohexanol in a 96 hour
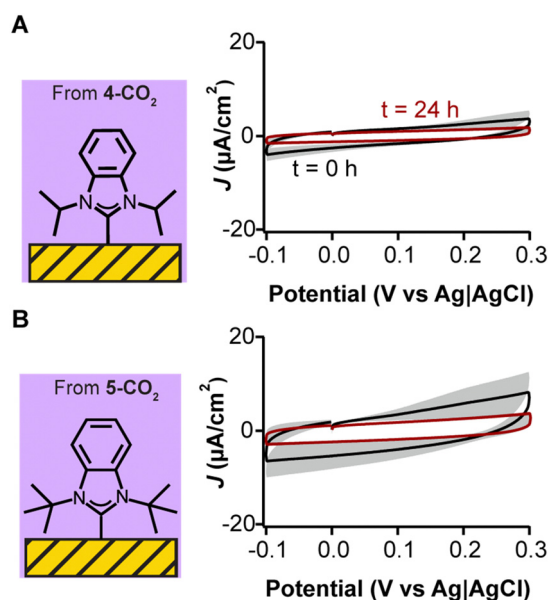

Fig. 5 Adlayers of NHC−CO₂ adducts do not show capacitive transitions. We illustrate this point here by showing cyclic voltammograms of adlayers made from NHC−CO₂ adducts containing either (A) isopropyl or (B) *tert*-butyl wingtips. The voltammograms are represented in terms of current density (μA cm^{-2}) and were recorded using a voltage scanning rate of 0.1 V s^{-1}. Solid lines represent the average of four modified electrodes, and the shaded areas represent their standard deviation.

experiment. Each adlayer was subjected to continuous voltammetric interrogation from 0.3 V to −0.4 V every 11 s for 96 h (Fig. 6). This voltage window covers the useful range of gold in physiological media, limited by surface oxidation at ≥ 0.3 V,[57,58] and oxygen reduction at ≤ -0.4 V.[59]

The MCH monolayer (Fig. 6A) showed flat capacitive currents over the first six hours of continuous interrogation, but started to quickly desorb after that period which was observed

as a linear increase in capacitive currents (orange trace in Fig. 6D). In contrast, both **(1-H)(OTf)** and **4-CO$_2$** showed decreases in capacitive currents over 96 hours (Fig. 6B and C). The capacitive current for **(1-H)(OTf)** dropped during the first hour before it plateaued for 60 hours, then very slowly increased towards the end of the experiment (green trace in Fig. 6D). We speculate the jump seen at ~68 h may be due to a power surge that affected the measurement. Nevertheless, the capacitive currents measured with **(1-H)(OTf)** are stable over periods longer than 60 h. The capacitive currents for **4-CO$_2$** plateaued within the first hour of continuous interrogation, and then remained completely stable until the end of our measurements (purple trace in Fig. 6D). These results unequivocally highlight the enhanced stability of NHC adlayers, especially **4-CO$_2$**, on gold relative to a benchmark thiol monolayer of mercaptohexanol and underscore their promise as passivating agents for electrochemical biosensor development.

Given that the strong σ-donation of NHCs is broadly applicable across transition metals and not exclusive to gold, we tested the ability of NHCs to form adlayers and passivate other important metal electrodes. Platinum and palladium electrodes are used in implantable continuous glucose monitors and other biosensing devices.[60–66] Likewise, the formation of chemisorbed NHC monolayers on platinum and palladium has also been confirmed by previous reports.[23,67–70] We employed platinum and palladium rod electrodes with similar dimensions as our gold electrodes (see Electrochemical methods in ESI† for details) and deposited both **(1-H)(OTf)** (Fig. 7E–H) and **4-CO$_2$** (Fig. 7I–L) with the same vacuum oven-based method described previously.

When interrogated *via* cyclic voltammetry, **4-CO$_2$** caused a significant dampening of capacitive currents, from 7.5 ± 1.4 μA

(Au), 11.4 ± 2.6 μA (Pt), and 5.5 ± 1.1 μA (Pd) down to 4.2 ± 1.2 μA, 3.4 ± 1.1 μA, and 1.2 ± 0.9 μA, respectively (Fig. 7I–K). **(1-H)(OTf)** resulted in a dampening of capacitive currents from 5.8 ± 3.0 μA (Au), 7.1 ± 1.8 μA (Pt), and 9.2 ± 4.1 μA (Pd) down to 2.9 ± 0.8 μA, 2.7 ± 0.7 μA, and 0.5 ± 0.09 μA (Fig. 7E–G). Indeed, the capacitive currents of the modified platinum and palladium electrodes were, in fact, lower than those achieved with gold electrodes, suggesting higher affinity for NHCs. We repeated these experiments using glassy carbon electrodes as control reasoning that the NHC carbon should not bind to the surface *via* a dative interaction. As expected, we observed no statistically significant effect on the capacitive currents of the glassy carbon electrodes (Fig. 7H and L). These combined results corroborate previous reports that demonstrated that NHCs form chemisorbed layers on gold, platinum, and palladium, but not on surfaces such as carbon. Additionally, they highlight the effectiveness of our deposition protocol at passivating metal electrodes other than gold.

Conclusions

We have investigated the effects of wingtip substituent and deposition method for NHCs when passivating gold electrode surfaces, and conducted preliminary evaluations of NHCs for the passivation of other biochemically important metal electrodes. Our results indicate that NHCs are a strong competitor for replacing thiols for the passivation of electrode surfaces in electrochemical biosensors. NHCs demonstrate comparable reductions of capacitive current *versus* a benchmark thiol
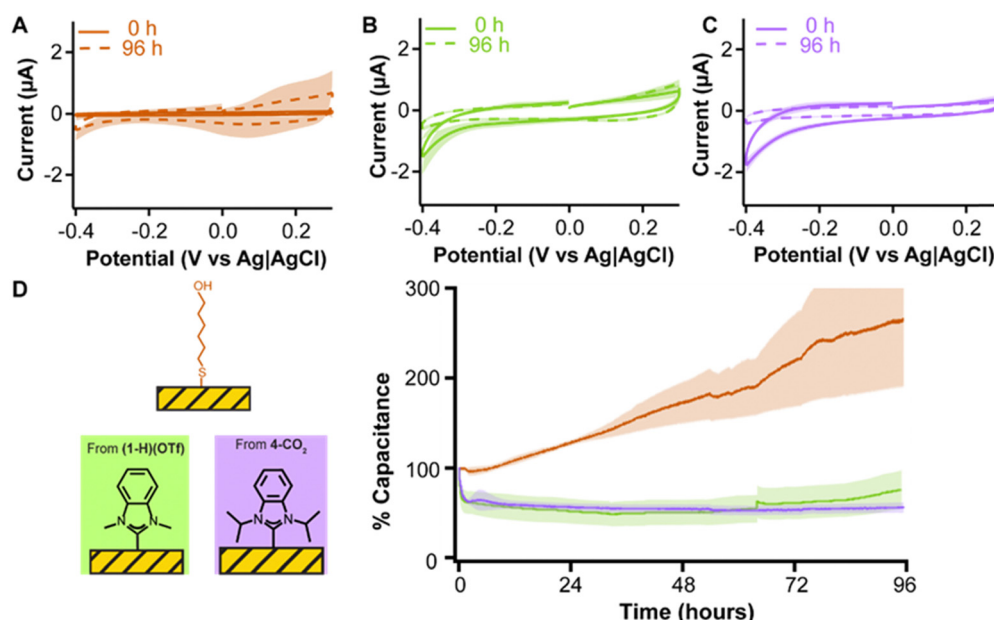

Fig. 6 Electrochemical probing of NHC stability compared to benchmark thiols. Electrodes functionalized with either (A) MCH, (B) **(1-H)(OTf)**, or (C) **4-CO$_2$** were cycled continuously for 96 h in voltammetric windows resulting in the reduction of oxygen (<0.25 V) and oxidation of gold (>0.3 V). (D) Capacitive current measurements at −0.05 V illustrate MCH monolayer degradation, represented by an increase in capacitance (orange trace). In contrast, **(1-H)(OTf)** (green trace) and **4-CO$_2$** (purple trace) adlayers improve over time. Lines represent the average of 4 electrodes with shaded regions as standard deviations.
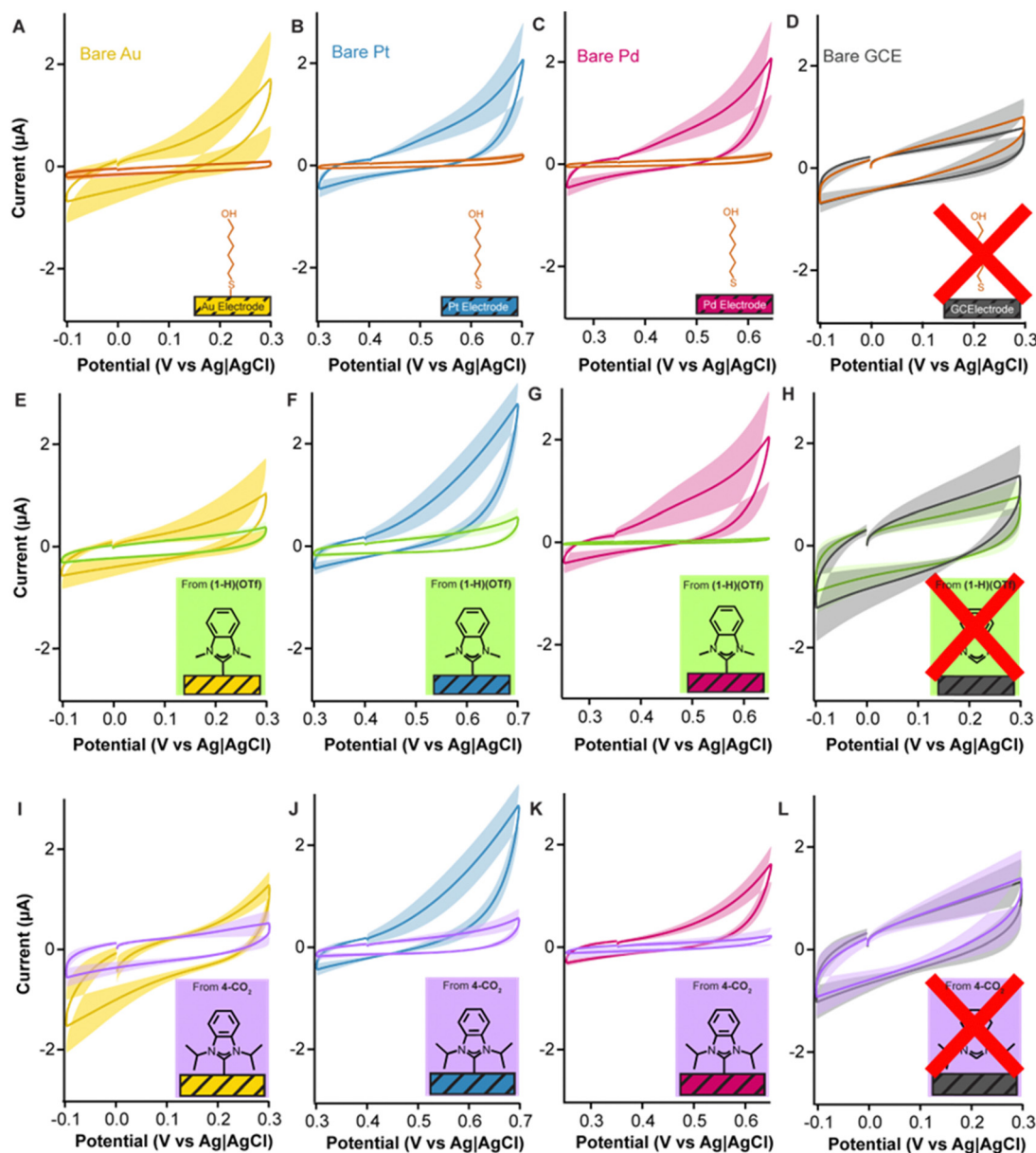
Fig. 7 Effects of deposition of MCH, (1-H)(OTf) and 4-CO$_2$ on four electrodes employed for biological applications. Mercaptohexanol deposition on (A) gold, (B) platinum, (C) palladium, and (D) glassy carbon is shown as a comparison. The deposition of (1-H)(OTf) resulted in the reduction of capacitive currents for (E) gold, (F) platinum, and (G) palladium electrodes. However, deposition on a negative control (H) glassy carbon electrode, which will not form a bond with the NHC, resulted in no changes in capacitive currents. The same trend is observed for 4-CO$_2$ on (I) gold, (J) platinum, (K) palladium, and (L) glassy carbon electrodes. Lines represent the average of 4 electrodes with shaded regions as standard deviations.

and, most critically, display significantly enhanced longevity under continuous cycling up to four days. This improved stability under continuous voltametric interrogation highlights NHC's utility against a key weakness of current SAM-based electrochemical biosensors: voltage-induced desorption of the monolayer.

Our wide-ranging study revealed the effects of variables of NHC wingtips and NHC precursors on the formation of adlayers on gold electrodes. Our results reaffirm that NHC–CO$_2$ adducts form superior monolayers on gold surfaces *versus* desorption from a benzimidazolium triflate salt. Additionally, our results highlight the importance of testing NHCs for purity

and to avoid cross contamination from anion exchange processes. Finally, we tested the most effective NHCs across common electrode materials for electrochemical sensors. Both platinum and palladium electrodes exhibited excellent passivation with a significant reduction in capacitive currents. However, as expected, no passivation was observed with glassy carbon electrodes.

Author contributions

I. M. J. performed ligand synthesis and spectroscopic characterization. V. C. performed electrochemical measurements. H.

L. K. assisted with ligand synthesis. N. A.-C. and D. M. J. designed and supervised the project. The manuscript was written by I. M. J., V. C., N. A.-C., and D. M. J.

Data availability

The data supporting this article have been included as part of the ESI.†

Conflicts of interest

There are no conflicts to declare.

Acknowledgements

References

1 A. M. Downs and K. W. Plaxco, *ACS Sens.*, 2022, **7**, 2823–2832.

2 J. Wu, H. Liu, W. Chen, B. Ma and H. Ju, *Nat. Rev. Bioeng.*, 2023, **1**, 346–360.

3 E. Hommel, B. Olsen, T. Battelino, I. Conget, I. Schütz-Fuhrmann, R. Hoogma, U. Schierloh, N. Sulli, H. Gough, J. Castañeda, S. de Portu, J. Bolinder and SWITCH Study Group, *Acta Diabetol.*, 2014, **51**, 845–851.

4 N. Arroyo-Currás, J. Somerson, P. A. Vieira, K. L. Ploense, T. E. Kippin and K. W. Plaxco, *Proc. Natl. Acad. Sci. U.S.A.*, 2017, **114**, 645–650.

5 A. M. Downs and K. W. Plaxco, *ACS Sens.*, 2022, **7**, 2823–2832.

6 N. J. Ronkainen, H. B. Halsall and W. R. Heineman, *Chem. Soc. Rev.*, 2010, **39**, 1747.

7 F. Li, Z. Yu, X. Han and R. Y. Lai, *Anal. Chim. Acta*, 2019, **1051**, 1–23.

8 J. Das, S. Gomis, J. B. Chen, H. Yousefi, S. Ahmed, A. Mahmud, W. Zhou, E. H. Sargent and S. O. Kelley, *Nat. Chem.*, 2021, **13**, 428–434.

9 V. Clark, K. Waters, B. Orsburn, N. N. Bumpus, N. Kundu, J. T. Sczepanski, P. Ray and N. Arroyo-Currás, *Angew. Chem.*, 2022, **134**, e202211292.

10 C. Parolo, A. Idili, G. Ortega, A. Csordas, A. Hsu, N. Arroyo-Currás, Q. Yang, B. S. Ferguson, J. Wang and K. W. Plaxco, *ACS Sens.*, 2020, **5**, 1877–1881.

11 Y. Xiao, A. A. Lubin, A. J. Heeger and K. W. Plaxco, *Angew. Chem., Int. Ed.*, 2005, **44**, 5456–5459.

12 A. Idili, C. Parolo, R. Alvarez-Diduk and A. Merkoçi, *ACS Sens.*, 2021, **6**, 3093–3101.

13 Y. Wu and N. Arroyo-Currás, *Angew. Chem., Int. Ed.*, 2024, **63**, e202312402.

14 A. Shaver, J. D. Mahlum, K. Scida, M. L. Johnston, M. Aller Pellitero, Y. Wu, G. V. Carr and N. Arroyo-Currás, *ACS Sens.*, 2022, **7**, 3895–3905.

15 A. Idili, J. Gerson, C. Parolo, T. Kippin and K. W. Plaxco, *Anal. Bioanal. Chem.*, 2019, **411**, 4629–4635.

16 A. Shaver and N. Arroyo-Currás, *Curr. Opin. Electrochem.*, 2022, **32**, 100902.

17 K. K. Leung, A. M. Downs, G. Ortega, M. Kurnik and K. W. Plaxco, *ACS Sens.*, 2021, **6**, 3340–3347.

18 Z. Watkins, A. Karajic, T. Young, R. White and J. Heikenfeld, *ACS Sens.*, 2023, **8**, 1119–1131.

19 A. Shaver, S. D. Curtis and N. Arroyo-Currás, *ACS Appl. Mater. Interfaces*, 2020, **12**, 11214–11223.

20 V. Clark, M. A. Pellitero and N. Arroyo-Currás, *Anal. Chem.*, 2023, **95**, 4974–4983.

21 N. Arroyo-Currás, *ACS Sens.*, 2024, **9**, 2228–2236.

22 N. Fontaine and P. Dauphin-Ducharme, *Curr. Opin. Electrochem.*, 2023, **41**, 101361.

23 C. A. Smith, M. R. Narouz, P. A. Lummis, I. Singh, A. Nazemi, C.-H. Li and C. M. Crudden, *Chem. Rev.*, 2019, **119**, 4986–5056.

24 G. Kaur, R. L. Thimes, J. P. Camden and D. M. Jenkins, *Chem. Commun.*, 2022, **58**, 13188–13197.

25 C. M. Crudden, J. H. Horton, I. I. Ebralidze, O. V. Zenkina, A. B. McLean, B. Drevniok, Z. She, H.-B. Kraatz, N. J. Mosey, T. Seki, E. C. Keske, J. D. Leake, A. Rousina-Webb and G. Wu, *Nat. Chem.*, 2014, **6**, 409–414.

26 L. M. Sherman, M. D. Finley, R. K. Borsari, N. Schuster-Little, S. L. Strausser, R. J. Whelan, D. M. Jenkins and J. P. Camden, *ACS Omega*, 2022, **7**, 1444–1451.

27 J. F. DeJesus, M. J. Trujillo, J. P. Camden and D. M. Jenkins, *J. Am. Chem. Soc.*, 2018, **140**, 1247–1250.

28 S. R. Thomas, W. Yang, D. J. Morgan, T. E. Davies, J. J. Li, R. A. Fischer, J. Huang, N. Dimitratos and A. Casini, *Chem. – Eur. J.*, 2022, **28**, e202201575.

29 S. R. Thomas and A. Casini, *J. Organomet. Chem.*, 2021, **938**, 121743.

30 N. A. Nosratabad, Z. Jin, L. Du, M. Thakur and H. Mattoussi, *Chem. Mater.*, 2021, **33**, 921–933.

31 R. M. Mayall, C. A. Smith, A. S. Hyla, D. S. Lee, C. M. Crudden and V. I. Birss, *ACS Sens.*, 2020, **5**, 2747–2752.

32 N. L. Dominique, A. Chandran, I. M. Jensen, D. M. Jenkins and J. P. Camden, *Chem. – Eur. J.*, 2024, **30**, e202303681.

33 M. A. Pellitero, I. M. Jensen, N. L. Dominique, L. C. Ekowo, J. P. Camden, D. M. Jenkins and N. Arroyo-Currás, *ACS Appl. Mater. Interfaces*, 2023, **15**, 35701–35709.

34 E. Amit, I. Berg, W. Zhang, R. Mondal, H. Shema, V. Gutkin, T. Kravchuk, F. D. Toste, Z. Nairoukh and E. Gross, *Small*, 2024, **20**, 2302317.

35 A. Inayeh, R. R. K. Groome, I. Singh, A. J. Veinot, F. C. De Lima, R. H. Miwa, C. M. Crudden and A. B. McLean, *Nat. Commun.*, 2021, **12**, 4034.

36 C. R. Larrea, C. J. Baddeley, M. R. Narouz, N. J. Mosey, J. H. Horton and C. M. Crudden, *Chem. Phys. Chem.*, 2017, **18**, 3536–3539.

37 R. L. Thimes, A. V. B. Santos, R. Chen, G. Kaur, L. Jensen, D. M. Jenkins and J. P. Camden, *J. Phys. Chem. Lett.*, 2023, **14**, 4219–4224.

38 G. Wang, A. Rühling, S. Amirjalayer, M. Knor, J. B. Ernst, C. Richter, H.-J. Gao, A. Timmer, H.-Y. Gao, N. L. Doltsinis, F. Glorius and H. Fuchs, *Nat. Chem.*, 2017, **9**, 152–156.

39 G. Lovat, E. A. Doud, D. Lu, G. Kladnik, M. S. Inkpen, M. L. Steigerwald, D. Cvetko, M. S. Hybertsen, A. Morgante, X. Roy and L. Venkataraman, *Chem. Sci.*, 2019, **10**, 930–935.

40 L. M. Sherman, S. L. Strausser, R. K. Borsari, D. M. Jenkins and J. P. Camden, *Langmuir*, 2021, **37**, 5864–5871.

41 L. Jiang, B. Zhang, G. Médard, A. P. Seitsonen, F. Haag, F. Allegretti, J. Reichert, B. Kuster, J. V. Barth and A. C. Papageorgiou, *Chem. Sci.*, 2017, **8**, 8301–8308.

42 M. J. Trujillo, S. L. Strausser, J. C. Becca, J. F. DeJesus, L. Jensen, D. M. Jenkins and J. P. Camden, *J. Phys. Chem. Lett.*, 2018, **9**, 6779–6785.

43 H. V. Huynh, T. T. Lam and H. T. T. Luong, *RSC Adv.*, 2018, **8**, 34960–34966.

44 N. Dordević and H. V. Huynh, *Organometallics*, 2022, **41**, 335–344.

45 T. Yoshida, M. Takeshita, H. Orita, N. Kado, S. Yasuda, H. Kato and Y. Itoh, *Chem. Pharm. Bull.*, 1996, **44**, 1128–1131.

46 M. Rodríguez-Castillo, D. Laurencin, F. Tielens, A. Van Der Lee, S. Clément, Y. Guari and S. Richeter, *Dalton Trans.*, 2014, **43**, 5978.

47 N. Hadei, E. A. B. Kantchev, C. J. O'Brie and M. G. Organ, *Org. Lett.*, 2005, **7**, 1991–1994.

48 D. M. Khramov and C. W. Bielawski, *J. Org. Chem.*, 2007, **72**, 9407–9417.

49 N. Arroyo-Currás, K. Scida, K. L. Ploense, T. E. Kippin and K. W. Plaxco, *Anal. Chem.*, 2017, **89**, 12185–12191.

50 A. J. Bard, L. R. Faulkner and H. S. White, *Electrochemical methods: fundamentals and applications*, Wiley, Hoboken, NJ, 3rd edn, 2022.

51 Q. Rayée, T. Doneux and C. Buess-Herman, *Electrochim. Acta*, 2017, **237**, 127–132.

52 X. Xu and C. L. Hussey, *J. Electrochem. Soc.*, 1992, **139**, 1295–1300.

53 Y. Hamasaki, N. Nakashima and Y. Niidome, *Chem. Lett.*, 2012, **41**, 962–964.

54 H. H. Hassan, M. A. M. Ibrahim, S. S. Abd El Rehim and M. A. Amin, *Int. J. Electrochem. Sci.*, 2010, **5**, 278–294.

55 K. Arai, F. Kusu, N. Noguchi, K. Takamura and H. Osawa, *Anal. Biochem.*, 1996, **240**, 109–113.

56 M. J. Trujillo, S. L. Strausser, J. C. Becca, J. F. DeJesus, L. Jensen, D. M. Jenkins and J. P. Camden, *J. Phys. Chem. Lett.*, 2018, **9**, 6779–6785.

57 J. Rodríguez-López, M. A. Alpuche-Avilés and A. J. Bard, *J. Am. Chem. Soc.*, 2008, **130**, 16985–16995.

58 Th Wink, S. J. Van Zuilen, A. Bult and W. P. Van Bennekom, *Analyst*, 1997, **122**, 43R–50R.

59 H. Yu, X. Li, T. Zhang, J. Liu, J. Tian and R. Yang, *ChemSusChem*, 2020, **13**, 2702–2708.

60 R. D. O'Neill, S.-C. Chang, J. P. Lowry and C. J. McNeil, *Biosens. Bioelectron.*, 2004, **19**, 1521–1528.

61 H. Karimi-Maleh, K. Cellat, K. Arıkan, A. Savk, F. Karimi and F. Şen, *Mater. Chem. Phys.*, 2020, **250**, 123042.

62 C. Kaewjangwad, S. Somsiri, S. Wangchuk, J. Saichanapan, K. Saisahas, K. Samoson, A. Soleh, K. Promsuwan and W. Limbut, *Electrochim. Acta*, 2024, **491**, 144292.

63 T. A. Peyser, K. Nakamura, D. Price, L. C. Bohnett, I. B. Hirsch and A. Balo, *Diabetes Technol. Ther.*, 2015, **17**, 548–554.

64 S. R. Chinnadayyala, J. Park, A. T. Satti, D. Kim and S. Cho, *Electrochim. Acta*, 2021, **369**, 137691.

65 C. Y. An, K. Zhuo, W.-J. Kim and C.-H. Chung, *Sens. Actuators, B*, 2015, **213**, 329–333.

66 M. J. L. Torre Poueymirou, R. Diaz Ayala and C. R. Cabrera, *Biophys. J.*, 2021, **120**, 366a.

67 T. Zhang, S. B. Khomane, I. Singh, C. M. Crudden and P. H. McBreen, *Phys. Chem. Chem. Phys.*, 2024, **26**, 4083–4090.

68 M. Koy, P. Bellotti, M. Das and F. Glorius, *Nat. Catal.*, 2021, **4**, 352–363.

69 S. Dery, I. Berg, S. Kim, A. Cossaro, A. Verdini, L. Floreano, F. D. Toste and E. Gross, *Langmuir*, 2020, **36**, 697–703.

70 S. Dery, S. Kim, G. Tomaschun, I. Berg, D. Feferman, A. Cossaro, A. Verdini, L. Floreano, T. Klüner, F. D. Toste and E. Gross, *J. Phys. Chem. Lett.*, 2019, **10**, 5099–5104.